IEEE Access
Multidisciplinary ⋮ Rapid Review ⋮ Open Access Journal

Received 29 May 2024, accepted 29 June 2024, date of publication 3 July 2024, date of current version 12 July 2024.

Digital Object Identifier 10.1109/ACCESS.2024.3422486

RESEARCH ARTICLE

Efficient Equivalent Circuits Model for Electric-LC Resonators in Periodic and Closed Waveguides

C. H. JOSEPH, (Member, IEEE), D. MENCARELLI, (Member, IEEE), L. PIERANTONI, (Senior Member, IEEE), P. RUSSO, (Senior Member, IEEE), AND L. ZAPPELLI, (Member, IEEE)

Dipartimento di Ingegneria dell'Informazione, Università Politecnica delle Marche, 60131 Ancona, Italy

Corresponding author: L. Zappelli (l.zappelli@univpm.it)

This work was supported by European Project Nanomaterials Enabling Smart Energy Harvesting for Next-Generation Internet-of-Things (NANO-EH) under Grant 951761 and Grant FETPROACT-EIC-05-2019.

ABSTRACT This paper details the extraction of possible equivalent circuits over a wide band for an Electric-LC resonator in two technological configurations: a) a multilayer stack working at mm-wave and b) a WR90 waveguide in the X band. The proposed equivalent circuits are based on a T structure or on only one shunt susceptance with two transmission lines. An identification process applied to the frequency behavior of the reactance/susceptance is used to obtain a more appropriate and efficient equivalent circuit, giving a physical meaning, if any, to each inductance, capacitance or resonator tank contained in the proposed circuits. Finally, experimental results are obtained for the ELC in the WR90 waveguide and used to identify an equivalent circuit able to represent also the effect of the material losses.

INDEX TERMS Compact circuit modeling, microwave and millimeter-wave circuits, model extraction of passive circuits, passive component modeling, periodic structures, waveguide structures.

I. INTRODUCTION

One of the problems in finding the equivalent circuit of microwave/mm wave structures is related to the complexity of the structure under study that could be obtained by combining several microwave discontinuities or other elements that could be recognized as inductors or capacitors. It is not easy to recognize an efficient equivalent circuit that takes into account each part of the complex device as an individual block as it occurs at low frequencies. Unfortunately, at a high frequency each component is made by distributed elements, except for some thin discontinuities in waveguide, as inductive or capacitive irises. Moreover, the measurement at microwaves are purely based on scattering parameters seen at the input and output ports and the complexity of the overall device is seen as a "black box" mixing the effect of each component that is represented by a 2×2 scattering matrix, with only three independent real parameters for a reciprocal lossless device ($|S_{11}|$, φ_{11}, φ_{22} for example). It is clear that the identification of the components of the "black box" is quite difficult starting from only three real parameters. The frequency behavior can help in the identification process but the problem is still complex, especially if transmission lines are contained in the overall device under test.

A first strategy in finding an equivalent circuit of the device under study could be based on the transformation of the 2×2 S-matrix in terms of a direct T or Π equivalent circuit by the usual transformation of the S matrix in Z or Y matrix [1], [2]. The obtained equivalent circuit is "minimal" in the sense that only three real parameters (reactances or susceptances) are used to represent the frequency behavior of the overall lossless circuit. The challenge now lies in identifying each reactance in terms of a capacitance or inductance combination that should have some physical meaning in relation to the blocks of the device under study. Synthesis based on poles and zeros for each reactance may be effective for low frequencies, but may not be suitable for extremely high frequencies, especially if transmission lines are present in the device.

The associate editor coordinating the review of this manuscript and approving it for publication was Ladislau Matekovits.

A second strategy is based on the identification of the S matrix in terms of the equivalent circuit for microwave discontinuities based on a shunt reactance with input and output transmission lines [1]. While the shunt susceptance represents the overall reflection and transmission properties of the device, the input and output transmission lines are used to change the phase properties of the equivalent circuit to match the prescribed phase of the scattering parameters of the device [3]. The shunt susceptance could be identified with the Brune synthesis. This second strategy could be useful to find a more compact and light equivalent circuit, as done in [4] for Split Ring Resonators (SRR), where the effect of the geometrical parameters on the circuital parameters is analyzed.

The proposed strategies will be applied to the analysis of ELC (Electric-LC) resonator in two different technological configurations: a) a multilayer dielectric stack, under the hypothesis of plane wave excitation incoming from the air and a periodic repetitions in the transverse section [5] and b) a WR90 waveguide operating in the X band, where the ELC is placed symmetrically in the longitudinal plane so that the electric field of the TE_{10} mode is parallel to the ELC plane. In the first case, the electromagnetic analysis is performed by applying the Floquet's boundary conditions, while in the second case, the usual modal propagation is used, defining electric boundary conditions in correspondence of the waveguide walls. In both cases, a numerical analysis is performed with the CST electromagnetic simulator.

ELC-based metamaterial resonators exhibiting negative permittivity offers several advantages such as a high level of symmetry in their geometry and negligible magnetoelectric coupling along with their ability to couple to both parallel and perpendicular components of an electric field [6], [7], [8], [9], [10], [11], [12], [13]. ELC resonators can be used in many scenarios, such as filtering structures [8], [9], [10], [11], [12], [13], [14], energy harvesting [15], sensors [16], [17], [18], [19], rasorbers [20]. Some literatures reported simple equivalent circuit approaches based on quasi-static analysis only to predict the resonance frequency for sub-wavelength resonators and not to predict the complete reflection/transmission behavior over a wide band [9], [12]. Moreover, the equivalent circuit approaches depends also from the kind of excitation applied to the resonators, as normal or oblique plane wave incidence on the ELCs plane [8], [9], [10], [11], [12], [13], [15], [20], [21], [22], [23], or lateral plane wave incidence [24], or an excitation with coplanar [25], [26] or microstrip [16], [17], [18], [19] transmission lines. In fact, in the presence of normal incidence, the ELCs can be correctly seen as a lumped load while for oblique incidence this approximation is still good only if the ELCs dimensions are small with respect to the wavelength. On the contrary, for lateral incidence or coplanar/microstrip transmission line excitation, the equivalent circuit should contain also some transmission lines to simulate the effect of the ELCs length in the direction of propagation of the exciting electromagnetic field. This effect could be neglected only for sub wavelength ELCs to define lumped equivalent circuits. The proposed approach in this paper works in analyzing precisely the reflection/transmission characteristics of the ELCs excited by a lateral plane wave incidence or placed along the longitudinal direction of a closed rectangular waveguide. The aim is to analyze the effects of the length of the ELCs on the equivalent circuit that is able to reproduce the ELCs electromagnetic properties over a large bandwidth, from micro/mm wave up to subTHz.

The presence of multiple resonances related to the dimensions of the ELC produce different frequency behavior, that can yield different equivalent circuits for similar geometries. In fact, we will show that, by increasing the side dimension of a square ELC in a WR90 waveguide, the behavior of the frequency response of the scattering parameters yield to an equivalent circuit that increases its complexity with the order (or kind) of the resonance. The first resonance will be identified with a very simple equivalent circuit over the whole X band, while the second one requires a more complex equivalent circuit that should take into account the effects of the longitudinal length of the ELC resonator with the presence of non-Foster reactive elements as negative inductances/capacitances. The proposed equivalent circuit can be a promising tool to improve the optimization process in the design of more complex filtering structures. This topic will be discussed with an example showing the improvement achievable in run time and also in the explanation of the frequency behavior of the global filtering structure.

Finally, the experimental results on the ELC in a WR90 waveguide will be used to define an equivalent circuit that takes into account also the presence of resistances related to the material losses.

II. THEORY

A. ELC IN DIELECTRIC STACK

As shown in Fig. 1(a), a plane wave propagating in the z direction with E_x and H_y components impinges from the air on a periodic distribution of a multilayer stack containing ELC's with periodicity of $L_x = 155\ \mu$m in the x direction and a periodicity of L_y in the vertical y direction with $L_y = h_{SiO_2} + h_{Si} = 310.19\ \mu$m. The multilayer stack has a length $L_s = 270\ \mu$m in the z direction. The single unit cell of the investigated ELC structure and the technology cross-section are displayed in Fig. 1(a) and 1(b). The ELC resonator is embedded in the SiO_2 layer (height $h_{SiO_2} = 10.19\ \mu$m) and deposited on top of a Silicon substrate with a height of $h_{Si} = 300\ \mu$m. The ELC structure has dimensions of $L = 150\,\mu$m, $w = 5\,\mu$m, $g = 5\ \mu$m and $h = 2\ \mu$m. A multilayer silicon technology stack has been considered for the analysis of ELC metacells as a possibility to utilize them in a real millimeter wave and sub-THz components and devices [27]. The reflection and transmission characteristics of this ELC

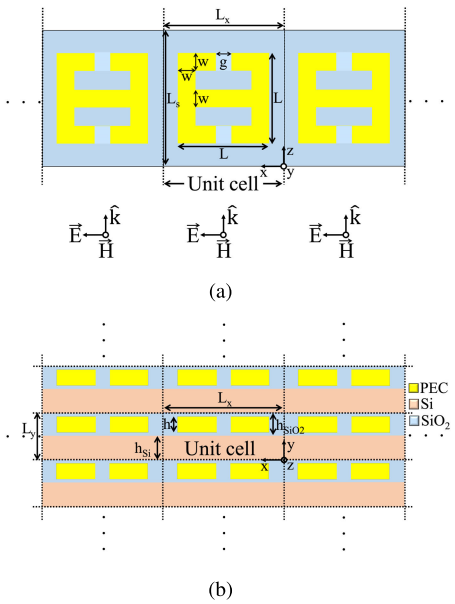

FIGURE 1. (a) Periodic arrangement of ELC resonators symmetrically placed in the unit cell. (b) Cross section of the multilayer high frequency technology stack (not in scale). The $L_x \times L_y$ unit cell is emphasized with dashed lines.

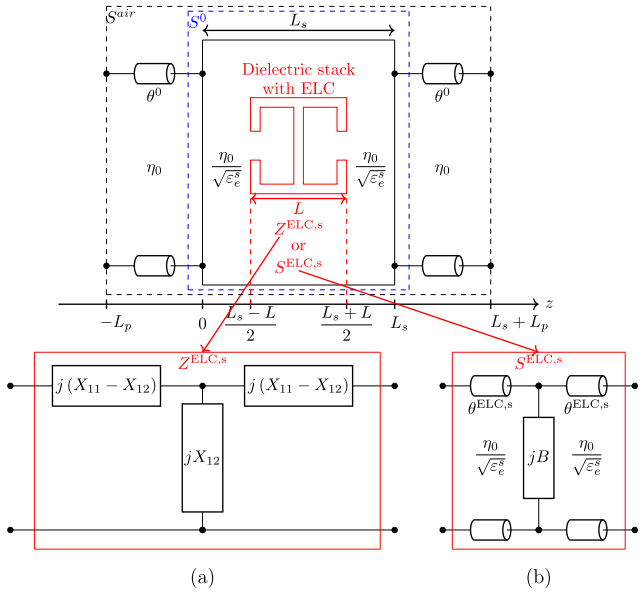

FIGURE 2. Two equivalent circuits representing the ELC resonator (a) by Z-matrix $Z^{\mathrm{ELC,s}}$ (b) by S-matrix $S^{\mathrm{ELC,s}}$.

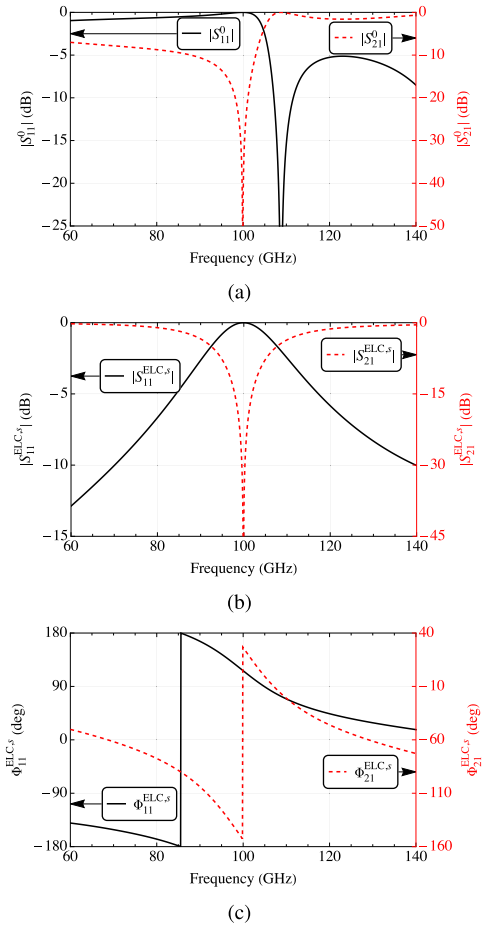

FIGURE 3. Scattering parameters seen at (see Fig. 2): (a) $z = 0^-, z = L_s^+$ (air, S^0) and (b)-(c) $z = \left(\frac{L_s - L}{2}\right)^-, z = \left(\frac{L_s + L}{2}\right)^+$ (ELC on the dielectric stack, $S^{\mathrm{ELC,s}}$).

resonator metacell has been studied with a Floquet ports arrangement and simulated using CST Microwave Studio.

Once the scattering matrix S^{air} of the structure has been obtained by CST (or by experimental results), we can define the two different equivalent circuits, shown in Fig. 2 of the "black box" represented by S^{air}. It should be recalled that the matrix S^{air} is the scattering matrix evaluated by considering two ports in the air, placed at $z = -L_{\mathrm{p}}$ and $z = L_s + L_{\mathrm{p}}$, as shown in Fig. 2, where L_{p} is the distance between the ports in the air and the front ($z = 0$) or back ($z = L_s$) face of the dielectric stack. To correctly evaluate the equivalent circuit of the ELC in the multilayer stack alone, we have to deembed S^{air} by eliminating the lengths L_{p}, i.e. the distance between the numerical ports and the position of the dielectric stack, to obtain the scattering matrix S^0 at the input and output sections at $z = 0$ and $z = L_s$ of the dielectric stack. The matrix S^0 takes into account both effects of (1) the discontinuity between the air and the dielectric stack and (2) the ELC placed symmetrically on the dielectric stack. To obtain the equivalent circuit of the ELC alone, we need to re-normalize S^0 with respect to the effective dielectric constant of the dielectric stack, that in our case is $\varepsilon_e^s = 11.64$, and de-embed the obtained scattering parameters to delete the effect of the stack length $\frac{L_s - L}{2}$, as shown in Fig. 2. In doing so, we obtain the scattering matrix of the ELC on the dielectric stack, $S^{\mathrm{ELC,s}}$, highlighted in red in Fig. 2.

The scattering parameters of S^0 and $S^{\mathrm{ELC,s}}$ are shown in Fig. 3: the main effect of the re-normalization is to delete the effect of the transition air-dielectric which "masks" the effective behavior of the ELC resonator. In fact, while the stop band frequency of the ELC at about 100 GHz is the same for S^0 and $S^{\mathrm{ELC,s}}$, the behavior of $|S_{11}|$ is different for the two cases: the re-normalization deletes the effect of the

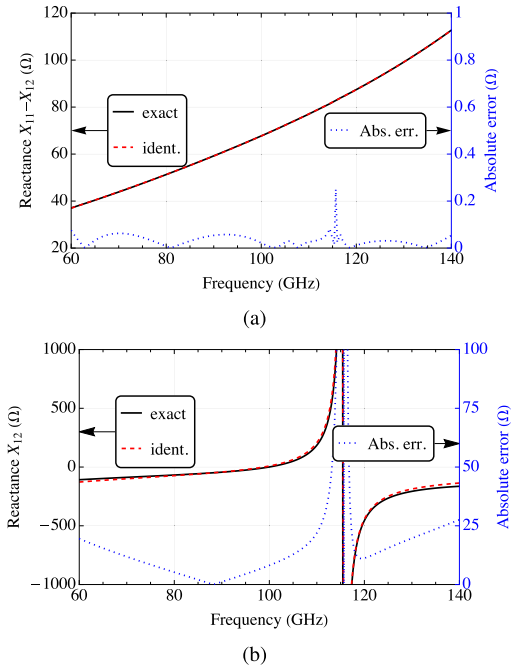

FIGURE 4. (a) Comparison between the series reactance $X_{11} - X_{12}$ extracted by $Z^{ELC,s}$ ("exact", black solid line, left axis) and that obtained by the two approximating series elements shown in Fig. 6(a) ("ident", red dashed line, left axis). (b) Comparison between the shunt reactance X_{12} extracted by $Z^{ELC,s}$ ("exact", black solid line, left axis) and that obtained by the two approximating series elements in Fig. 6(a) ("ident", red dashed line, left axis). Absolute errors between exact and identified values are shown in the right axes (dotted blue line).

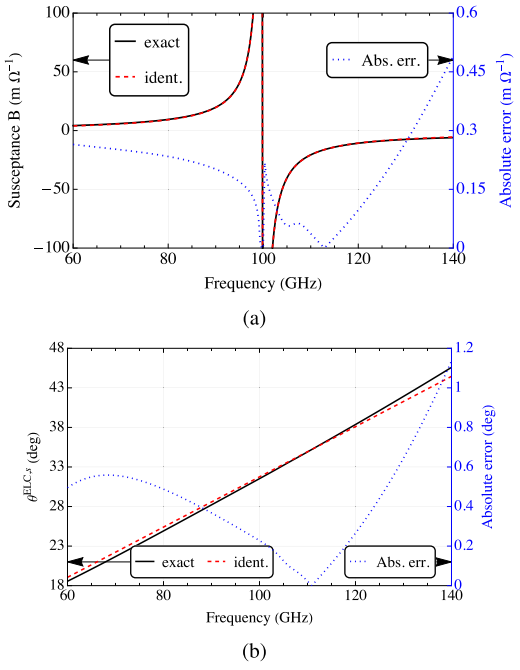

FIGURE 5. (a) Comparison between the shunt susceptance extracted by $S^{ELC,s}$ with (1) ("exact", black solid line, left axis) and that obtained by two approximating shunt branches shown in Fig. 7(a) ("ident", red dashed line, left axis). (b) Comparison between the electrical length of the transmission lines extracted by $S^{ELC,s}$ ("exact", black solid line, left axis) and that obtained by setting an equivalent length $L_e = 77.5$ μm ("ident", red dashed line, left axis). Absolute errors between exact and identified values are shown in the right axes (dotted blue line).

length along z of the stack that produces a good matching at about 110 GHz. By doing so, we have highlighted the actual behavior of the ELC resonator shown in Fig. 3(b)-3(c), where Φ_{ij} represent the phase of the scattering coefficients. At this stage, one can proceed to obtain the two possible equivalent circuits shown in Figs. 2(a)-2(b).

The first T circuit, Fig. 2(a), is obtained by a simple transformation of $S^{ELC,s}$ in the corresponding Z matrix, while the second circuit, Fig. 2(b), is based on the circuits used by [1], [2] for 2-port devices, by evaluating

$$B = \pm 2 \frac{\left|S_{11}^{ELC,s}\right|}{\eta_s \left|S_{21}^{ELC,s}\right|} \tag{1}$$

$$\theta^{ELC,s} = -\frac{1}{2} \arg\left(S_{11}^{ELC,s} \frac{2j - B\eta_s}{2j}\right) \tag{2}$$

with $S_{11}^{ELC,s} = S_{22}^{ELC,s}$ by symmetry of the device and $\eta_s = \frac{\eta_0}{\sqrt{\varepsilon_e^s}}$ [3].

The evaluated reactances for the ELC equivalent circuit of Fig. 2(a) are shown in Fig. 4 (black solid lines, "exact", left axis), while the shunt susceptance and the electrical length of the transmission line for the ELC equivalent circuit of Fig. 2(b) are shown in Fig. 5 (black solid lines, "exact", left axis). The two different circuits produce two different readings of their overall behavior. In fact, while both representations give an immediate reading of the presence of zero of transmission (the zero value of X_{12} or the pole of B produces a short circuit at about 100 GHz), the reading of X_{11}, X_{12} is more complex. In fact, the origin of the pole at about 115 GHz in X_{12}, Fig. 4(b), is due to the denormalization process of $S^{ELC,s}$ which produces an impedance matrix $Z^{ELC,s}$ that is singular at this frequency. In fact, it is well known that, while the scattering matrix of a device is always defined and never singular, the same does not occur for the impedance matrix that could be singular at some frequencies: $jX_{11}, jX_{12} \to \infty$. Hence the presence of the singularity of X_{12} has no physical meaning, being not related to the physical behavior of the ELC. Moreover, the singularity of X_{11}, X_{12} disappear in $X_{11} - X_{12}$ because the two singularities cancel each other as discussed in the Appendix. Hence, the series reactance $X_{11} - X_{12}$ becomes regular without singularity. From this point of view, the representation in terms of the equivalent circuit in Fig. 2(b), where the shunt susceptance B becomes singular exactly at the ELC resonant frequency, seems more appropriate, efficient and correctly defines the physical behavior of the resonator.

To obtain a more powerful circuit representation of the ELC behavior over a wide band, we need to apply an identification process of the frequency behavior to both proposed equivalent circuits and try to give a physical explanation to the obtained circuit elements. To do this, a classic identification process based on the analysis of poles and zeros of the reactances/susceptances of Fig. 2

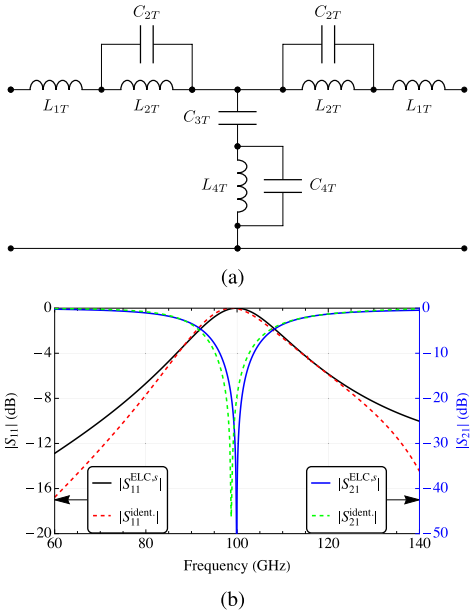

FIGURE 6. (a) Identified approximated circuits for the circuit in Fig. 2(a) obtained by the impedance matrix $Z^{\mathrm{ELC,s}}$. (b) Comparison between the amplitudes of $S^{\mathrm{ELC,s}}$ and the scattering parameters obtained by the approximated circuit shown in Fig. 6(a).

has been applied to obtain a good fitting. In particular, a rational function representing a possible fitting circuit, including negative inductances and capacitances if any [4], is minimized with respect to the exact values shown with black continuous lines in Figs. 4 or 5(a). Once the coefficient of the numerator and denominator of the rational function have been obtained, they are matched with series or shunt inductances/capacitances or LC (tank) resonant circuits. The circuit configuration identifying the circuit obtained by the $Z^{\mathrm{ELC,s}}$ matrix in Fig. 2(a) is shown in Fig. 6(a) with $L_{1T} = 24.46$ pH, $L_{2T} = 69.15$ pH, $C_{2T} = 6.21$ fF, $C_{3T} = 17.97$ fF, $L_{4T} = 38.85$ pH, $C_{4T} = 48.86$ fF.

The comparison between the exact behavior of the reactances obtained by $Z^{\mathrm{ELC,s}}$ and the approximated one obtained by the identified circuit in Fig. 6(a) are shown in Fig. 4 for the series and shunt reactances of the T circuit with a good agreement between the exact (black solid lines, "exact", left axis) and the approximated identified values (red dashed lines, "ident.", left axis). The absolute error between the exact and the identified values of the reactances is shown with dotted blue lines (right axis) in Fig. 4. The error is very low over the whole band, except for X_{12} near the resonance at 115 GHz, where a small error in the identification of the resonance frequency can cause an error increasing. From the identified values of the reactance, we can evaluate the corresponding identified scattering parameters, $S_{ij}^{\mathrm{ident.}}$, that are compared with the exact values in Fig. 6(b). The comparison is good in the band of 80–120 GHz, with a little shift in the resonant frequency and maximum absolute error of about 4 dB at 140 GHz for $|S_{11}|$ (maximum percentage error about 42 %).

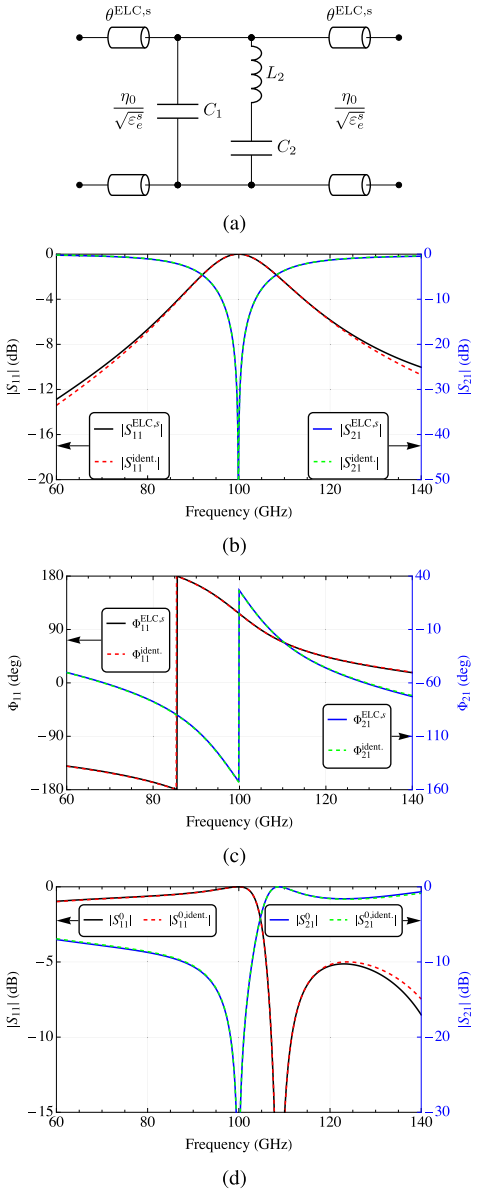

FIGURE 7. (a) Identified approximated circuits for the circuit in Fig. 2(b) obtained by the scattering matrix $S^{\mathrm{ELC,s}}$. (b)-(c) Comparison between the amplitudes/phases of $S^{\mathrm{ELC,s}}$ and the scattering parameters obtained by the approximated circuit shown in Fig. 7(a). (d) Comparison between the amplitudes of S^0 and the scattering parameters obtained by the approximated circuit shown in Fig. 7(a) embedded in the dielectric stack between $z = 0^-, z = L_S^+$ (see Fig. 2).

The same identification process has been applied to the shunt susceptance of the circuit of Fig. 2(b), obtaining the circuit configuration shown in Fig. 7(a), with $C_1 = 0.41$ fF, $L_2 = 0.37$ nH, $C_2 = 6.87$ fF. The comparison between the exact values of B and its identified circuit is very good, as shown in Fig. 5 (black solid and red dashed lines, left axis). The absolute error between them is shown with dotted blue lines (right axis) and is very low over the whole band. The comparison between the the scattering parameters obtained by the exact values extracted by $S^{\mathrm{ELC,s}}$ with (1) and the approximated value obtained by the two shunt branches is

shown in Fig. 7(b)-7(c) with a very good agreement between the exact (black solid line, "exact") and the approximated values (red dashed line, "ident.") over the whole band, with maximum absolute error 0.67 dB for $|S_{11}|$ (max. percentage error 6%) and 0.063 dB for $|S_{21}|$ (max. percentage error 5%). Similarly, the electrical length of the lines $\theta^{\mathrm{ELC,s}}$ obtained by $S^{\mathrm{ELC,s}}$ can be approximated with an equivalent length $L_e = 77.5\,\mu$m, with a very good agreement as shown in Fig. 5(b) (Absolute error less than 0.15 degrees , dotted blue lines, right axis). L_e is slightly larger than $L/2 = 75\,\mu$m and this is due to the effect of the ELC that produces a larger path for the incident, reflected and transmitted waves with respect to the nominal one. Anyway L_e still maintains a very good approximation for the phase of the scattering parameters of $S^{\mathrm{ELC,s}}$, as shown in Fig. 7(c). This can be confirmed by the reconstruction of the scattering parameters of the global structure seen at the air-dielectric stack interface ($z = 0^-, z = L_s^+$ in Fig. 2). In fact, Fig. 7(d) shows that the comparison between the exact values and those obtained by the equivalent circuit in Fig. 7(a) imbedded in the dielectric stack between $z = 0^-, z = L_s^+$ is very good over the whole band, with maximum absolute error 1.02 dB for $|S_{11}|$ (max. percentage error 15%) and 0.11 dB for $|S_{21}|$ (max. percentage error 12%). This comparison could not be so good if also the identified phases in the equivalent circuit were not correct.

Finally, it should be interesting to give a physical explanation of the identified circuit in Fig. 7(a). The presence of the second branch with the tank L_2C_2 is clearly related to the resonant LC behavior, given by the capacitance of the ELC gap and the ELC inductance, while the first branch with C_1 is due to interactions between the ELC conductors.

On the contrary, the X_{12} resonant tanks contained in the T identified circuit in Fig. 6(a) is related to the singularity of the $Z^{\mathrm{ELC,s}}$ matrix at about 115 GHz, obtained by the transformation of $S^{\mathrm{ELC,s}}$ in $Z^{\mathrm{ELC,s}}$, while the tank contained in the series branch, resonating at about 340 GHz, comes from the requirement of a good identification for $X_{11} - X_{12}$ that the pure inductance L_{1T} cannot ensure. Moreover, their resonant frequency is not related to the reflection or transmission properties of the ELC but, at the same time, their presence must ensure that X_{12} has a zero at 100 GHz, i.e. the resonant frequency of the ELC, where total reflection occurs.

Summing up, the identified circuit shown in Fig. 7(a) seems more reasonable and with a physical meaning more robust with respect to the T identified circuit in Fig. 6(a).

B. ELC IN WR90 RECTANGULAR WAVEGUIDE

The second configuration analyzed is a rectangular WR90 waveguide loaded with a square ELC resonator designed on a lossless FR4 substrate as shown in Fig. 8. The substrate is placed symmetrically with respect to the horizontal x-direction. For this case, the chosen dimensions are: $a = 22.86\,\mathrm{mm}, b = 10.16\,\mathrm{mm}, L = 4.67\,\mathrm{mm}, L_{\mathrm{tc}} = 0.835\,\mathrm{mm}, L_d = 20\,\mathrm{mm}, w = 1\,\mathrm{mm}, g = 1.5\,\mathrm{mm}, t = 1.6\,\mathrm{mm}$. The equivalent circuit proposed for this configuration is similar to that used in the previous

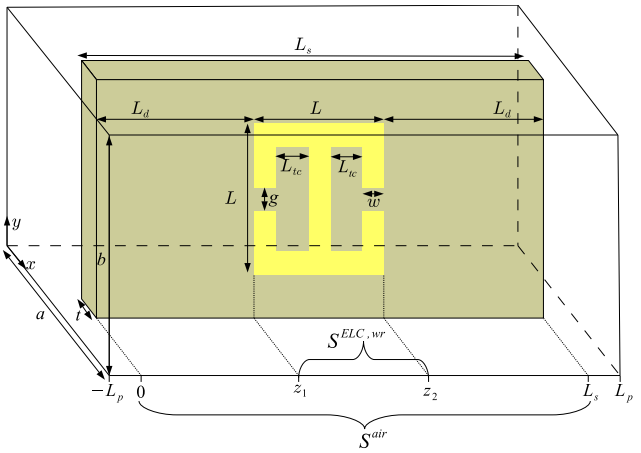

FIGURE 8. Rectangular waveguide loaded with a square ELC placed on a dielectric substrate (not in scale).

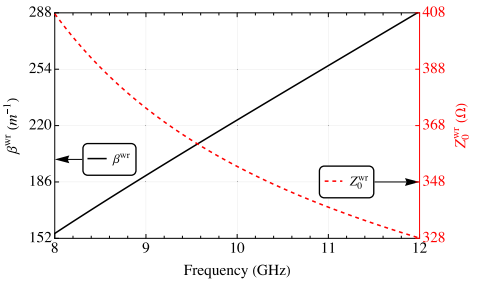

FIGURE 9. WR90 waveguide loaded with lossless FR4 substrate: propagation constant of the fundamental mode β^{wr} (black solid line) and modal impedance Z_0^{wr} (red dashed line).

sub-section, shown in Fig. 2(b). The T circuit is not analyzed for this case because we have shown in the previous section that its evaluation and identification can be cumbersome due to the singularity of its Z matrix.

The propagation constant β^{wr} of the fundamental mode of the WR90 waveguide loaded with the substrate and the modal impedance, Z_0^{wr}, are shown in Fig. 9. They are used to renormalize and de-embed the scattering parameters seen from the air at $z = 0^-$ and $z = L_s^+$ to obtain those seen in the dielectric loaded waveguide, exactly at the boundary of the ELC resonator, i.e. $z = z_1^-, z = z_2^+$, as shown in Fig. 8. The scattering parameters amplitudes seen in the waveguide from the air at $z = 0^-$ and $z = L_s^+$, S^{air}, and those seen at the ELC boundaries in the dielectric, $S^{\mathrm{ELC,wr}}$, are shown in Fig. 10(a)-10(b), respectively.

Following the same procedure of the previous sub-section, we can obtain the electrical parameters of the equivalent circuit of Fig. 2(b). In fact, the exact values of the electrical length of the transmission lines, $\theta^{\mathrm{ELC,wr}}$, and the susceptance B can be obtained by (1)-(2) where η_s must be replaced by the dispersive modal impedance Z_0^{wr} (Fig. 9). The electrical length of the equivalent circuit in Fig. 7(a), $\theta^{\mathrm{ELC,wr}}$, is shown in Fig. 11 (black solid lines "exact", left axis), together with the identified values (red dashed lines "ident", left axis). For this case, the electrical length $\theta^{\mathrm{ELC,wr}}$ can be identified

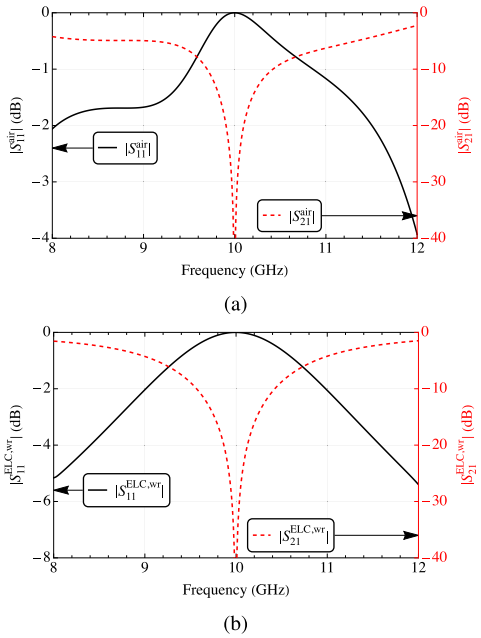

FIGURE 10. Scattering parameters amplitude seen at: (a) $z = 0^-, z = L_s^+$ (S^{air}) and (b) $z = z_1^-, z = z_2^+$ ($S^{ELC,wr}$). Longitudinal planes are shown in Fig. 8.

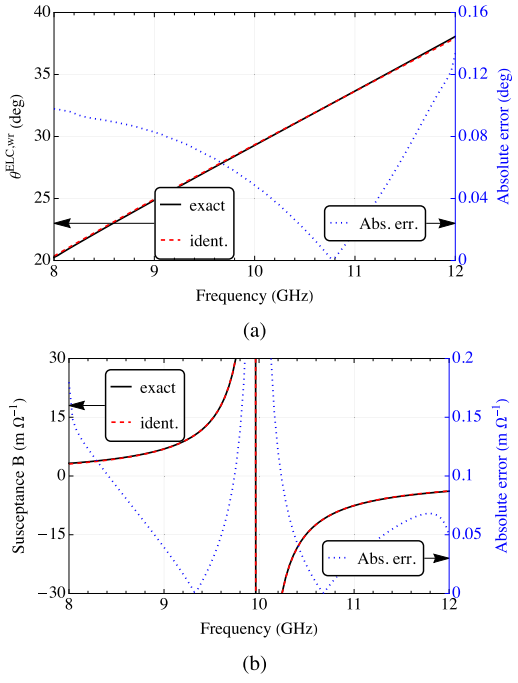

FIGURE 11. Exact and identified values (left axis) and their absolute error (right axis) of the elements of the equivalent circuit shown in Fig.2(b) and 7(a) for WR90 waveguide loaded with one ELC on a FR4 substrate: (a) electrical lengths of the transmission lines; (b) shunt susceptance.

with an equivalent FR4 loaded WR90 waveguide of length $L_e = 2.29$ mm, which is very close to $L/2 = 2.335$ mm. The absolute error between the exact and identified values is less than 0.15 degrees (dotted blue lines, right axis).

Similarly, in Fig. 11(b) we report the exact values of B (black solid lines, "exact", left axis) and the corresponding

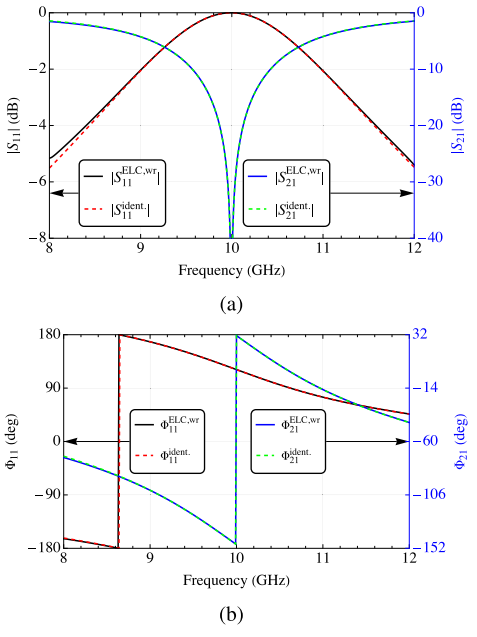

FIGURE 12. Comparison between $S^{ELC,wr}$ and the scattering parameters obtained by the circuit in Fig. 7(a) whose values are shown in Fig. 11.

ones obtained by the identified values (red dashed lines, "ident", left axis) ($C_1 = 0.805$ fF, $L_2 = 10.934$ nH, $C_2 = 23.187$ fF in the equivalent circuit of Fig. 7(a)). An excellent agreement is obtained as highlighted by the absolute error (dotted blue lines, right axis in Fig. 11) that is less than 0.2 m Ω^{-1} in the whole band (apart near the resonance where a small error in the identified resonant frequency can cause an error increasing).

The scattering parameters obtained by the identified equivalent circuit, $S_{ij}^{ident.}$ (red and green dashed lines), are compared with the exact ones (black and blue solid lines) in Fig. 12 with very good agreement in both amplitude and phase (maximum absolute error 0.35 dB for $|S_{11}|$ and 0.14 dB for $|S_{21}|$; maximum percentage error 6% and 8% respectively). Hence, the equivalent circuit proposed in Fig. 7(a) seems to be a valid approximation also for a WR90 waveguide loaded with ELC on FR4 substrate in the X band.

Other two structures with smaller ELC lengths have been analyzed with the proposed equivalent circuit and they are described as cases b and c in Tab. 1 (the first row describes the case just discussed). The obtained electric parameters for the equivalent circuits are shown in the Table and the corresponding results are shown in Fig. 13 with a very good agreement between exact and identified scattering parameters (Fig. 13(a): maximum absolute error 1.97 dB for $|S_{11}|$ and 0.004 dB for $|S_{21}|$; maximum percentage error 7% and 9% respectively; Fig. 13(c): maximum absolute error 1.02 dB for $|S_{11}|$ and 0.008 dB for $|S_{21}|$; maximum percentage error 5% and 8% respectively.).

On the other hand, it could be interesting to understand how effective could be the identification of one ELC in WR90 waveguide with the very simple circuit shown in Fig. 7(a) by enlarging the dimensions of the ELC. This can be done

TABLE 1. Geometric and electric parameters of the analyzed structures resonating at 10 GHz. L, w, g, L_e expressed in mm, capacitances in fF, inductances in nH.

case	L	$\frac{L}{\lambda_g}$	w	g	L_e	L_1	C_1	L_2	C_2
a	4.67	0.166	1	1.5	2.29	0	1.41	10.9	23.2
b	2.8	0.099	0.2	0.03	1.43	0	1.02	71.6	3.5
c	2.4	0.085	0.1	0.003	1.23	0	1.01	146.5	1.7
d	6.22	0.221	1	1.5	8.73	-21.1	-24.4	231.4	1.1

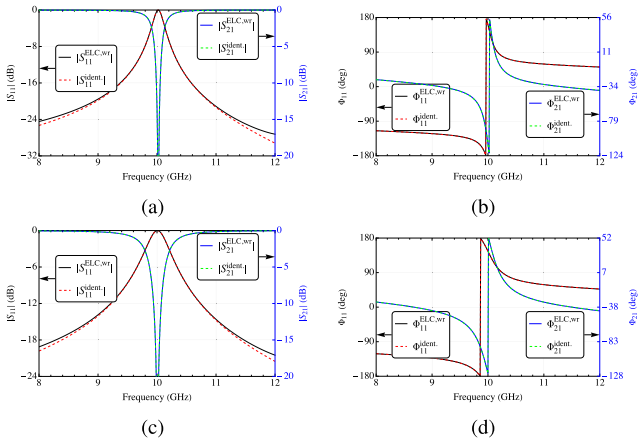

FIGURE 13. Comparison between $S^{ELC,wr}$ and the scattering parameters obtained by the equivalent circuit of Fig. 7(a) with the identified values shown in Tab. 1 for cases a and b.

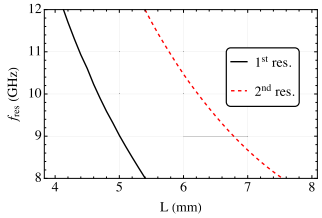

FIGURE 14. Resonance frequency of one square ELC in WR90 waveguide by varying the external side L.

by analyzing the variations in the resonance frequency by altering the length of the sides in the square ELC (g and w are fixed as the case a in Table 1), as shown in Fig. 14. It is evident that increasing the dimensions of the ELC a second resonance appears. It should be interesting to understand if the previous simple equivalent circuit can still be a good approximation of the actual behavior of the ELC resonator at the second resonance. To do this, we have applied the previous identification process to the scattering parameters of an ELC with $L = 6.22$ mm, resonating at about 10 GHz as in the previous case.

The main difference between the two resonances is in the electromagnetic field distribution around the ELC structure. In fact, if we compare the electromagnetic field maps for the two analyzed cases of ELC ($L = 4.67$ or 6.22 mm) shown in Fig. 15, we can notice that the main effect of the resonance is a very strong electric field for the shorter ELC with side $L = 4.67$ mm and a very strong magnetic field for the larger ELC with side $L = 6.22$ mm. Therefore, the length of the ELC resonator produces an effect in terms of resonating

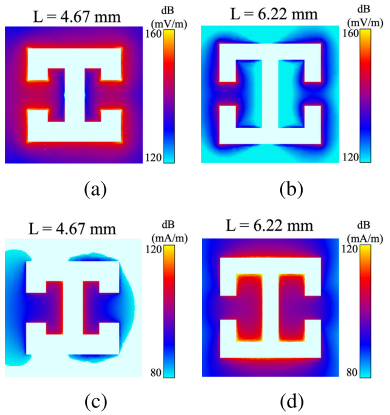

FIGURE 15. Amplitude of: (a)-(b) electric field and (c)-(d) magnetic field for the two ELCs with side 4.67 mm or 6.22 mm at the resonance frequency.

electromagnetic field that will change the identification of the shunt susceptance.

In fact, we have at first identified the electric parameters of the circuit of Fig. 7(a) previously used, obtaining $C_1 = 26.45$ fF, $L_2 = 0.21$ μH, $C_2 = 1.18$ fF. The comparison between the exact (black solid line) and the identified results (blue dotted line) are shown in Fig. 16(a). It is evident that the proposed identified equivalent circuit based on a capacitance and a LC resonating tank accurately reproduces the correct results within a narrow bandwidth around the resonance frequency, while in the previous case (Figs. 12–13, smaller ELCs) the comparison was very good over the whole bandwidth with the same kind of identified elements. The main difference between the larger and the smaller ELCs is that the exact susceptance of the larger ELC shows a non-Foster behavior ($dB(f)/df < 0$) in the lower (8-9.5 GHz) and upper (10.5-12 GHz) parts of the band. Hence, to improve the identification of the non-Foster parts of the susceptance we have to add some non-Foster elements, such as negative inductances and/or capacitances. In doing so, we can identify a new circuit similar to that shown in Fig. 7(a), where the first branch is replaced by a non-Foster L_1C_1 tank. From the identification process, we obtain the following values for the new components, $L_1 = -21.14$ nH, $C_1 = -24.36$ fF, $L_2 = 0.23$ μH, $C_2 = 1.09$ fF (case d, Table 1), and the identified results (red dashed line) are shown in Fig. 16(a) obtaining a very good agreement with the exact results (black solid line). The absolute error between the exact and identified values (dotted orange line, right axis) is very low over the whole band.

The effect of the ELC length is appreciable also on the transmission line electrical length shown in Fig. 16(b). In fact, in this case the behavior of $\theta^{ELC,wr}$ is a non linear function (black solid line, "exact") that can be approximated with the linear one satisfying the minimum distance in terms of least square mean (red dashed line, "ident."). The equivalent length of the transmission line with linear behavior is $L_e = 8.73$ mm, which is much larger than $L/2 = 3.11$ mm

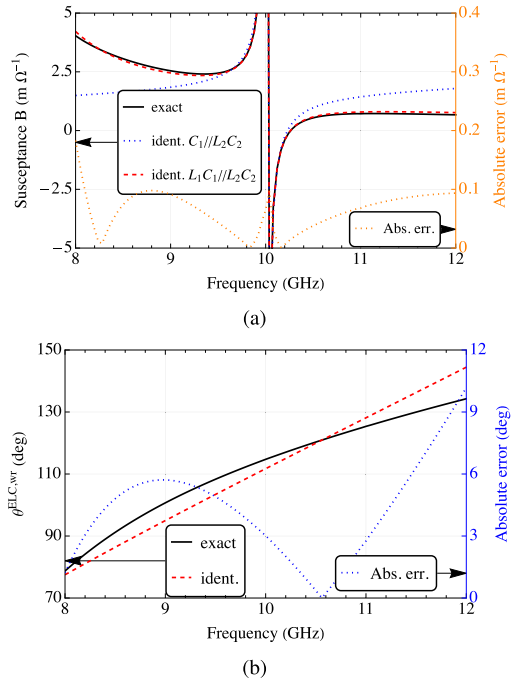

FIGURE 16. WR90 waveguide loaded with one square ELC on a FR4 substrate with $L = 6.22$ mm: exact and identified values (left axis) and their absolute error (right axis) of the (a) shunt susceptance and (b) electrical lengths of the transmission lines.

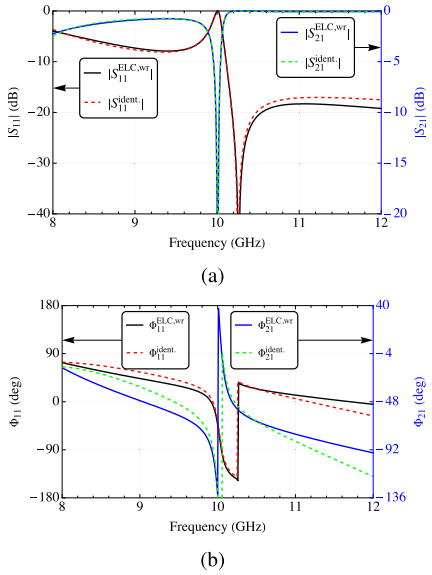

FIGURE 17. WR90 waveguide loaded with one square ELC on a FR4 substrate with $L = 6.22$ mm: comparison between $S^{ELC,wr}$ and the scattering parameters obtained by the equivalent circuit of Fig. 7(a) with the identified values shown in Fig. 16.

other than what happens for the first resonance. The absolute error between the exact and identified values is acceptable over the whole band (dotted blue line, right axis).

The comparison between the exact values of the scattering parameters and those obtained with the non-Foster identified circuit and the equivalent transmission line of length $L_e = 8.73$ mm are shown in Fig. 17(a)-17(b) with a very good agreement for the amplitude over the whole bandwidth (maximum absolute error 2.35 dB for $|S_{11}|$ and 0.21 dB for $|S_{21}|$; maximum percentage error 9% and 14%, respectively) and a good agreement also for the phase.

Summing up, for all the cases referring to the first resonance (cases a-c of Table 1) with a ratio $\frac{L}{\lambda_g}$ less than 0.17 evaluated at 10 GHz, the equivalent circuit can be summarized with a very good approximation by two transmission lines, each of length $L_e \approx L/2$, surrounding a lumped load with two shunt branches made by a pure capacitance and an LC tank. For a larger ratio $\frac{L}{\lambda_g}$, the ELC have a different behavior related to the presence of a second resonance that changes the identified equivalent circuit. In fact, the two transmission lines are greater than $L/2$ while the shunt load requires the presence of non-Foster elements to correctly reproduce the frequency behavior of the ELC scattering parameters over the whole band.

C. APPLICATION OF THE EQUIVALENT CIRCUIT

The proposed equivalent circuit can be used in an optimization process with many advantages with respect to pure numerical optimization by electromagnetic simulators. Just as an example, let's suppose we want to enlarge the stop band of the ELC at the first resonance in the range 9.5-10 GHz. The simplest solution is to design a new ELC resonating at 9.5 GHz and to put in cascade with ELC resonating at 10 GHz. This is not sufficient because we have also to choose the distance d between the ELCs to obtain the best results in terms of bandwidth. This could be done numerically by CST but the main problem is the run time required to perform such optimization. In fact, the run time required for just one simulation varies from about 5 minutes for $d = 5$ mm to about 8 minutes for $d = 25$ mm. The optimization process requires tens of simulations and the run time could be very long. To shorten the run time we could evaluate the scattering parameters (and consequently the obtained stop band) for a number of cases, for example from $d = 5$ mm to $d = 20$ mm with a step of 1 mm (16 cases), and choose the distance ensuring the largest stop band in this set of simulations. This strategy requires about 80-90 min to solve all cases.

The use of the equivalent circuit reduces drastically the run time for the optimization. In fact, once obtained the equivalent circuit for the new 9.5 GHz ELC (as discussed in the previous sub-section) we can cascade it with the equivalent circuit of the 10 GHz ELC by inserting between them a transmission line of electrical length $\beta^{wr}d$ representing the waveguide loaded with FR4, as shown in Fig. 18(a). Hence, the scattering parameters can be easily obtained with the classical evaluation of the input impedance of the overall equivalent circuit shown in Fig. 18(a) [1], [2] when it is closed at the left/right port with the modal impedance Z_0^{wr}. The evaluation of the scattering parameters and their stop band for the previous 16 cases is very fast, about 1.5 sec for each value of d, for total time of about 24 sec

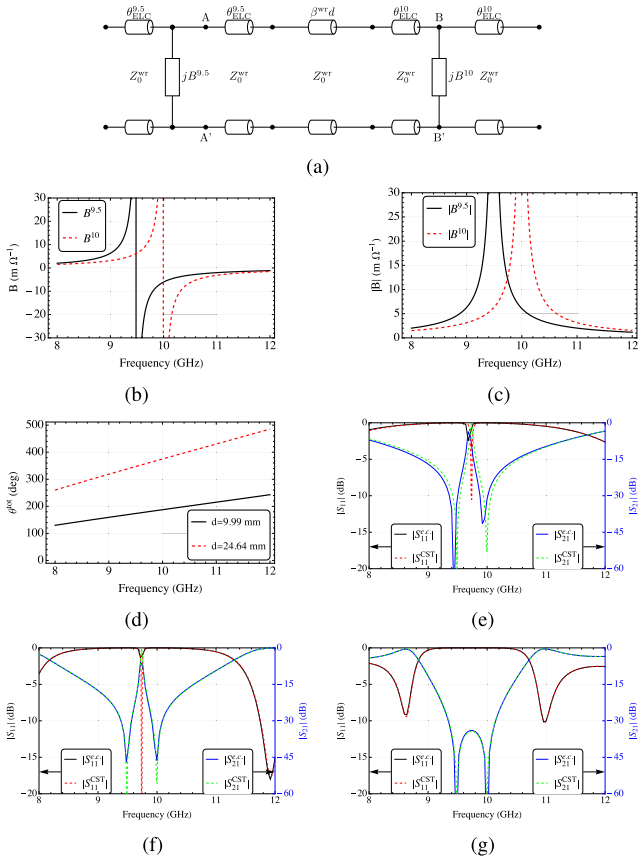

FIGURE 18. (a) Overall equivalent circuit of the cascade of two ELCs resonating at 9.5 and 10 GHz; (b)-(c) behavior of the susceptances $B^{9.5}$, B^{10}; (d) total electrical length comprised between $B^{9.5}$ and B^{10} for d=9.99 or 24.64 mm; (e)-(f) scattering parameters of the cascade of two ELCs for d=9.99 or 24.64 mm; (g) scattering parameters of the cascade of two ELCs for the optimized value d = 17 mm.

against 80 min with CST. It is clear that the equivalent circuit approach becomes a winning strategy in the optimization procedure.

The use of the equivalent circuit approach is useful also to refine the range where the best solution for d must be searched. In fact, in Fig. 18(a) the transmission lines of the equivalent circuits of the two ELCs and the transmission line of the connecting section can be put together to obtain only one overall transmission line with electrical length $\theta_{tot} = \theta^{9.5}_{ELC} + \beta d + \theta^{10}_{ELC}$. In order to evaluate S_{11}, the circuit shown in Fig. 18(a) must be closed on the modal impedance $Z_0^{\rm wr}$ at the right port. The transmission line at the right end, between jB^{10} and the right port, is transparent being closed on the modal impedance. Hence $Z_0^{\rm wr}$ is directly in shunt with jB^{10}. The behavior of $B^{9.5}$, B^{10} are shown in Fig. 18(b) while their amplitudes in Fig. 18(c). The direct comparison between the amplitudes shows that at about 9.75 GHz the two susceptances have the same value but with different sign (B^{10} capacitive, $B^{9.5}$ inductive). If the total length θ_{tot} is equal to a multiple of π at this frequency, the input admittance seen at section A-A' is equal to the admittance seen at section B-B', i.e. $1/Z_0^{\rm wr} + jB^{10}$. At this frequency $B^{10} = -B^{9.5}$ and the global admittance seen at the input section becomes $Y_{\rm in} = jB^{9.5} + jB^{10} + 1/Z_0^{\rm wr} = 1/Z_0^{\rm wr}$ with perfect matching. This means that at this frequency the stop band behavior is "broken" and the goal to obtain a stop band between 9.5 and 10 GHz is not reached. To verify the presence of perfect matching at 9.75 GHz we must evaluate the distance d that gives perfect matching at the input port. To do this, we need the values of $\beta^{\rm wr}, \theta^{9.5}_{ELC}, \theta^{10}_{ELC}$ at 9.75 GHz: $\beta^{\rm wr} = 214.4\ {\rm m}^{-1}, \theta^{9.5}_{ELC} = 0.51$ rad, $\theta^{10}_{ELC} = 0.49$ rad. Hence the electrical length of the waveguide connecting the two ELCs to obtain perfect matching must be $\beta^{\rm wr} d = \pi - (\theta^{9.5}_{ELC} + \theta^{10}_{ELC}) = 2.14$ rad. Hence, $d = \frac{2.14}{214.4} + k\frac{\lambda}{2} = (9.99 + k\ 14.65)$ mm where k is an integer that takes into account the periodicity of the transmission line. Hence, we can expect that choosing d=9.99 mm and d=9.99+14.65=24.64 mm we have perfect matching at 9.75 GHz. This is confirmed by the plot of the global electrical length (in degrees) for d=9.9 mm and d=24.64 mm in Fig. 18(d): it is evident that at 9.75 GHz the total electrical length is just 180° or 360° and hence perfect matching is obtained, being at this frequency $B^{10} = -B^{9.5}$. Hence the global stop band width, expected to be comprised between 9.5 and 10 GHz for the presence of the two resonating ELCs, is "broken" by the perfect matching frequency at 9.75 GHz as shown in Fig. 18(e)-18(f) for d=9.99 and 24.64 mm. In the same figures, the comparison with the results obtained by CST is shown with dashed lines. This preliminary discussion helps us also to define the range to find the optimized value of d to obtain a large stop band. In fact, the range is just comprised between 9.99 and 24.64 mm, where perfect matching occurs at 9.75 GHz. If we would use directly CST, we can limit the search of the optimized value lowering the global run time (many minutes, may be hours), while using our equivalent circuit approach the run time is just tens seconds. The cascade results for the best case ($d = 17$ mm) are shown in Fig. 18(g).

This analysis shows how the proposed equivalent circuit could be an interesting tool in optimization process.

III. EXPERIMENTAL RESULTS

The two ELCs resonating at the first and second resonances have been fabricated on a lossy FR4 substrate and are shown in Fig. 19(a), according to the dimensions reported in Tab.1, cases a and d. The details of the ELC designed at the first resonance are shown in Fig. 19(b), where the upper ruler has a step between two adjacent ticks equal to 0.5 mm. The lower step is in inches. The correct placement in the waveguide has been obtained by using the red spacer shown in Fig. 19(c), realized with a 3D printer, with horizontal dimension equal to $\frac{a-t}{2}$, vertical dimension less than b, and longitudinal dimension greater than L_s (see Fig. 8). The spacer has been placed in the waveguide and the substrate with the ELC has been inserted in the waveguide and laid to the spacer. Then, the spacer has been easily moved toward the end of the waveguide (due to a vertical dimension less than b, the spacer can be easily moved along the longitudinal dimension).

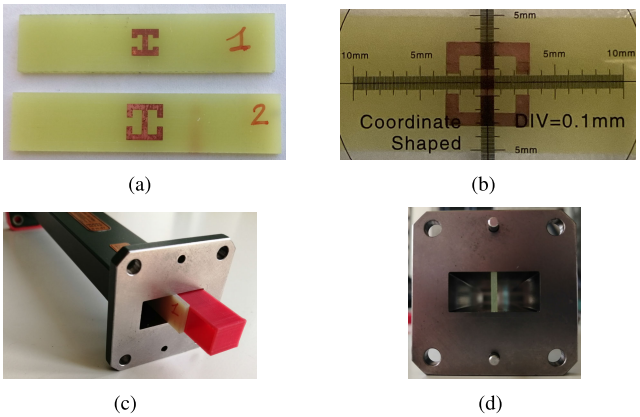

FIGURE 19. (a) Realized ELC for the first and second resonances. (b) Detail of the ELC for the first resonance. (c) Use of the spacer for the placement of the dielectric substrate. (d) Placement of the dielectric substrate in the WR90 waveguide.

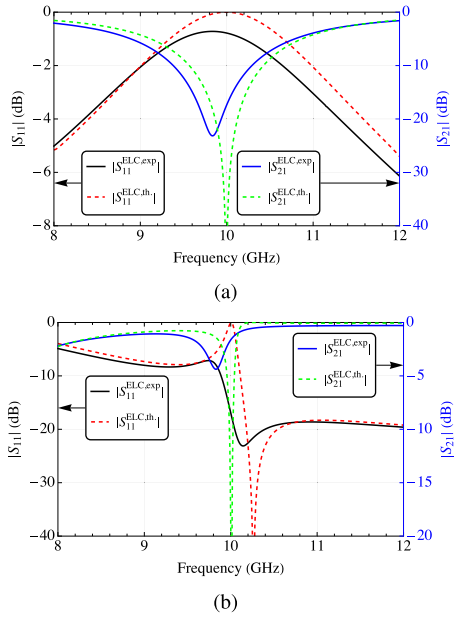

FIGURE 20. Comparison between experimental ("exp") and theoretical ("th") results for the ELC designed at the first (a) and second (b) resonance.

The final placement of the substrate is shown in Fig. 19(d) with a precision of about ±0.02 mm.

The scattering parameters of the waveguide loaded with the ELC have been measured with E8361A PNA Keysight Network Analyzer. As in the theoretical analysis, the scattering parameters have been renormalized with respect to the modal impedance of the substrate and de-embedded to obtain the scattering parameters seen at the input and output sections of the ELC. The comparison between the experimental values and the theoretical values obtained in Sub-Section II-B are shown in Fig. 20(a)-20(b) for both resonators. The presence of the lossy substrate which could have different electrical characteristics with respect to that used in the simulation and the effect of a mechanical precision of about ±0.02 mm in the copper layout moved the resonance

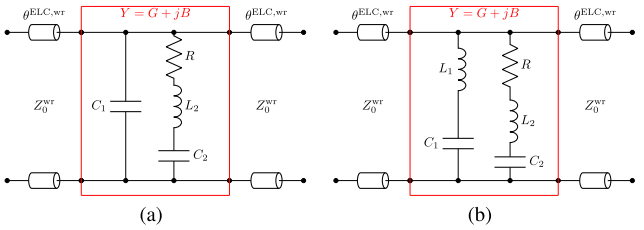

FIGURE 21. Identified approximated circuits for the lossy case of an ELC resonator placed on a substrate in WR90 waveguide at: (a) first resonance ($L = 4.67$ mm) (b) second resonance ($L = 6.22$ mm).

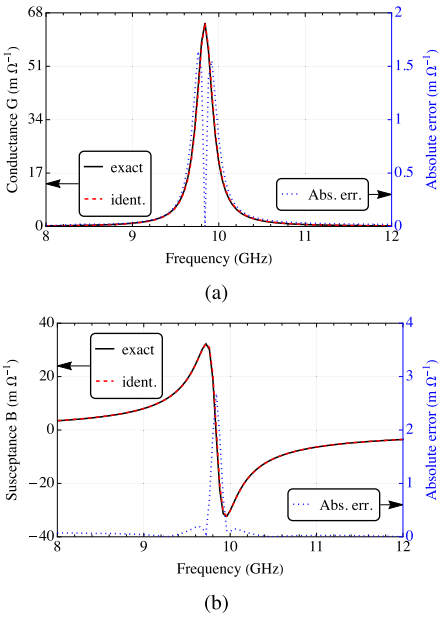

FIGURE 22. Exact and identified values (left axis) and their absolute error (right axis) of the elements of the equivalent circuit shown in Fig. 21(a) for WR90 waveguide loaded with one ELC on a FR4 lossy substrate for the first resonance: (a) shunt conductance and (d) shunt susceptance.

at about 9.8 GHz for both the resonators while the theoretical value was 10 GHz. While the first resonator shows a behavior very similar to the theoretical case, the second resonator has a different behavior around the resonance frequency while is very similar at the ends of the frequency band.

The first lossy resonator has been analyzed with the same approach as of Sub-Section II-B with the only difference that the equivalent circuit must contain a complex admittance $Y = G + jB$ instead of the pure susceptance B, as shown in Fig. 21(a). The complex admittance Y has been identified with $C_1 = 0.96$ fF, $R = 15.43\ \Omega$, $L_2 = 11.13$ nH, $C_2 = 23.51$ fF. The resistance takes into account the material losses. The obtained values are very similar to those evaluated for the lossless case discussed in Sub-Section II-B, apart from the value of the resistance. These values have been used to evaluate the identified complex admittance Y that is compared in Fig. 22(a)-22(b) with the exact values extracted by the scattering parameters, showing a very good agreement. Similarly, the comparison between the scattering parameters obtained with the identified circuit and the experimental values is shown in Fig. 23 (maximum absolute error 0.12 dB for $|S_{11}|$ and 1.2 dB for $|S_{21}|$; maximum percentage error 2%

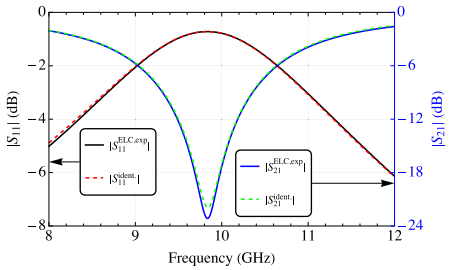

FIGURE 23. Comparison between the amplitudes of $S^{ELC,wr}$ and the scattering parameters obtained by the lossy equivalent circuit of Fig. 21(a).

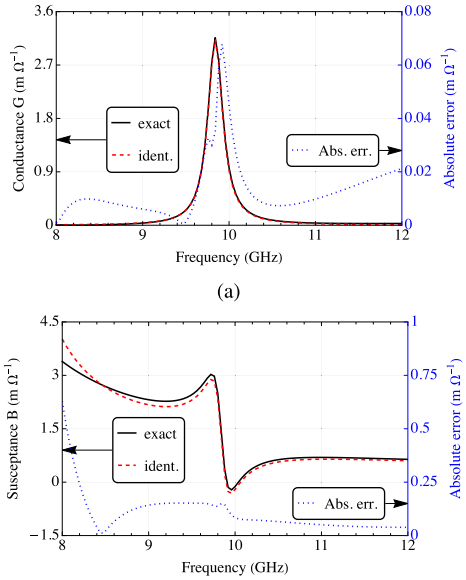

FIGURE 24. Exact and identified values (left axis) and their absolute error (right axis) of the elements of the equivalent circuit shown in Fig.21(b) for WR90 waveguide loaded with one ELC on a FR4 lossy substrate for the second resonance: (a) shunt conductance and (d) shunt susceptance.

and 6%, respectively). This implies that the identified lossy circuits very well match the experimental results.

Regarding the lossy ELC at the second resonance, more complex circuit shown in Fig. 21(b) must be used to identify its global complex admittance shown in Fig. 24 with black solid lines. In fact, the presence of non-Foster behavior in the lower and higher parts of the band imply the presence of negative inductances/capacitances other than a resistance to take into account the material losses. The identified values are: $L_1 = -27.11$ nH, $C_1 = -18.03$ fF, $R = 319.67\ \Omega$, $L_2 = 0.247\ \mu$H, $C_2 = 1.055$ fF. These values have been used to evaluate the identified complex admittance Y shown in Fig. 24 (red dashed line) with a very good agreement with the exact values. The absolute error for the conductance is acceptable over the whole band (dotted blue line, right axis) while for the susceptance a low peak appear near the frequency with maximum slope near the resonant frequency. Finally, the scattering parameters obtained by the identified equivalent circuit are compared in

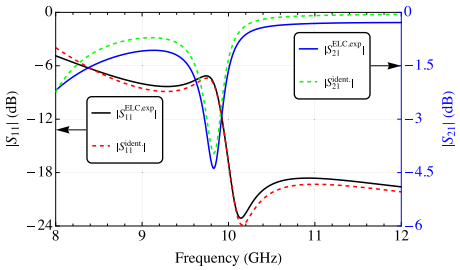

FIGURE 25. Comparison between the amplitudes of $S^{ELC,wr}$ and the scattering parameters obtained by the lossy equivalent circuit of Fig. 21(b) for WR90 waveguide loaded with one ELC on a FR4 lossy substrate for the second resonance.

Fig. 25 with the exact values, showing again a very good agreement (maximum absolute error 1.1 dB for $|S_{11}|$ and 0.43 dB for $|S_{21}|$; maximum percentage error 18% and 26%, respectively).

IV. CONCLUSION

Two possible equivalent circuits have been proposed and analyzed for an ELC resonator in a multi-stack dielectric substrate. The two circuits are obtained by the Z or S matrices of the device under study. An identification process based on the analysis of poles and zeros has been applied to the reactances/susceptance of the proposed equivalent circuits, showing a good agreement with the extracted values. The analysis of the identified series/shunt branches yields to define the circuit based on only one susceptance as more efficient and with a physical meaning. Then the ELC resonator has been placed in a rectangular waveguide and the efficiency of the equivalent circuit based on only one susceptance has been discussed, showing that this simple circuit is able to correctly reproduce the behavior over the whole band for the ELC designed at the first (electric) resonance by means of an identified circuit based on a shunt between a capacitance and an LC tank. On the other hand, the simple circuit must be replaced with a more complex one, containing also non-Foster elements, if we want to obtain a good comparison for an ELC designed at the second (magnetic) resonance. Finally, experimental results have been discussed and two lossy equivalent circuits have been proposed showing a very good agreement for the ELC at both resonances.

APPENDIX A
IMPEDANCE MATRIX OF A TWO-PORT RECIPROCAL SYMMETRIC DEVICE

Given the S matrix of a reciprocal ($S_{21} = S_{12}$) and symmetric ($S_{22} = S_{11}$) device

$$S = \begin{bmatrix} S_{11} & S_{12} \\ S_{12} & S_{11} \end{bmatrix} \tag{A.1}$$

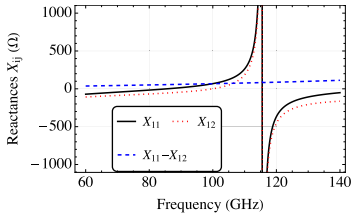

FIGURE 26. Frequency behavior of the reactances of the ELC on the dielectric stack.

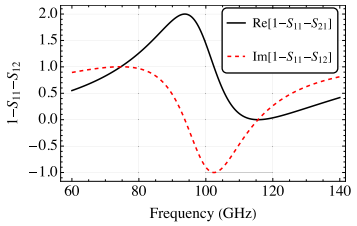

FIGURE 27. Frequency behavior of $1 - S_{11} - S_{12}$ to verify condition (A.7).

the impedance matrix Z is [1], [2]:

$$Z = Z_0\,[I - S]^{-1} \cdot [I + S] = \begin{bmatrix} Z_{11} & Z_{12} \\ Z_{12} & Z_{11} \end{bmatrix} \tag{A.2}$$

being Z_0 the normalization impedance and

$$\begin{aligned} Z_{11} &= Z_0 \frac{1 - S_{11}^2 + S_{12}^2}{(1 - S_{11} - S_{12})(1 - S_{11} + S_{12})} \\ &= Z_0 \frac{1 + S_{11} - S_{12}}{1 - S_{11} + S_{12}} + z_{12} \end{aligned} \tag{A.3}$$

$$Z_{12} = Z_0 \frac{2S_{12}}{(1 - S_{11} - S_{12})(1 - S_{11} + S_{12})} \tag{A.4}$$

The series impedance in the T circuit shown in Fig. 2(a) is equal to

$$Z_s = Z_{11} - Z_{12} = Z_0 \frac{1 + S_{11} - S_{12}}{1 - S_{11} + S_{12}}. \tag{A.5}$$

From (A.3)-(A.4), Z_{11} and Z_{12} are singular at the frequency f_0 where

$$S_{12} = \pm(1 - S_{11}) \tag{A.6}$$

while the series impedance (A.5) is singular only if

$$S_{12} = -(1 - S_{11}) \tag{A.7}$$

because Z_{11} and Z_{12} cancel their singularities if $S_{12} = 1 - S_{11}$.

Hence, while the shunt impedance Z_{12} is always identified by LC circuit (tank) resonating at the frequency f_0 where (A.6) is satisfied for any sign, the series impedance Z_s has two different circuit identifications:

1) if $S_{12} = S_{11} - 1$ at f_0, the series impedance Z_s is singular ($Z_s \to \infty$) and identified by LC tank resonating at the same frequency of Z_{11}, Z_{12};
2) if $S_{12} = 1 - S_{11}$ at f_0, the series impedance Z_s is not singular ($Z_s \to Z_0 \frac{S_{11}}{1 - S_{11}}$) and identified by a combination of inductances/capacitances, as discussed in Sec. II-A.

The scattering matrix of the ELC analyzed in Sec. II-A is characterized by the frequency behavior shown in Fig. 3(b)–3(c). Being lossless the ELC, the impedance matrix is purely imaginary, hence $Z_{11} = jX_{11}, Z_{12} = jX_{12}$, and X_{11}, X_{12} become singular at about $f_0 = 115$ GHz, as shown in Fig. 26 (black solid and dotted red lines). On the other hand, S_{11}, S_{12} satisfy condition 2) at $f_0 = 115$ GHz, as shown in Fig. 27. Hence the series reactance $X_{11} - X_{12}$ cancels the singularity of X_{11}, X_{12} and becomes regular at $f_0 = 115$ GHz, as shown in Fig. 26 (dashed blue line).

REFERENCES

[1] N. Marcuvitz, *Waveguide Handbook*. New York, NY, USA: McGraw-Hill, 1951.

[2] C. G. Montgomery, R. H. Dicke, and E. M. Purcell, *Principles of Microwave Circuits*. London, U.K.: Institution of Electrical Engineers, 1987.

[3] L. Zappelli, "Simple, fast, and effective identification of an equivalent circuit of a waveguide junction with *N* ports," *IEEE Trans. Microw. Theory Techn.*, vol. 63, no. 1, pp. 48–55, Jan. 2015.

[4] C. H. Joseph, D. Mencarelli, L. Pierantoni, P. Russo, and L. Zappelli, "Identification of compact equivalent circuit model for metamaterial structures," *IEEE Trans. Antennas Propag.*, vol. 71, no. 7, pp. 5850–5864, Jul. 2023.

[5] H. J. Christopher, D. Mencarelli, L. Pierantoni, P. Russo, and L. Zappelli, "Efficient equivalent circuits approach for millimeter wave metamaterial resonators," in *IEEE MTT-S Int. Microw. Symp. Dig.*, Jun. 2023, pp. 103–106.

[6] D. Schurig, J. J. Mock, and D. R. Smith, "Electric-field-coupled resonators for negative permittivity metamaterials," *Appl. Phys. Lett.*, vol. 88, no. 4, Jan. 2006, Art. no. 041109.

[7] H. Odabasi, F. L. Teixeira, and D. O. Guney, "Electrically small, complementary electric-field-coupled resonator antennas," *J. Appl. Phys.*, vol. 113, no. 8, Feb. 2013, Art. no. 084903.

[8] Q. H. Sun, Q. Cheng, H. S. Xu, B. Zhou, and T. J. Cui, "A new type of band-pass FSS based on metamaterial structures," in *Proc. Int. Workshop Metamaterials*, Nov. 2008, pp. 267–269.

[9] W. Withayachumnankul, C. Fumeaux, and D. Abbott, "Compact electric-LC resonators for metamaterials," *Opt. Exp.*, vol. 18, no. 25, pp. 25912–25921, Dec. 2010.

[10] W. Withayachumnankul, C. Fumeaux, and D. Abbott, "Planar array of electric-*LC* resonators with broadband tunability," *IEEE Antennas Wireless Propag. Lett.*, vol. 10, pp. 577–580, 2011.

[11] T. D. Karamanos, A. I. Dimitriadis, and N. V. Kantartzis, "Compact double-negative metamaterials based on electric and magnetic resonators," *IEEE Antennas Wireless Propag. Lett.*, vol. 11, pp. 480–483, 2012.

[12] A. Dhouibi, S. N. Burokur, A. de Lustrac, and A. Priou, "Comparison of compact electric-LC resonators for negative permittivity metamaterials," *Microw. Opt. Technol. Lett.*, vol. 54, no. 10, pp. 2287–2295, Oct. 2012.

[13] S. Bhattacharyya, H. Baradiya, and K. V. Srivastava, "An ultra thin metamaterial absorber using electric field driven LC resonator with meander lines," in *Proc. IEEE Int. Symp. Antennas Propag.*, Jul. 2012, pp. 1–2.

[14] M. Aldrigo, L. Zappelli, A. Cismaru, M. Dragoman, S. Iordanescu, D. Mladenovic, C. Parvulescu, D. Vasilache, C. H. Joseph, D. Mencarelli, L. Pierantoni, and P. Russo, "Fast method for the assessment of SRR or ELC-based planar filters: Numerical analysis and experiments," *IEEE Access*, vol. 11, pp. 77307–77323, 2023.

[15] A. A. G. Amer, S. Z. Sapuan, N. Nasimuddin, A. Alphones, and N. B. Zinal, "A comprehensive review of metasurface structures suitable for RF energy harvesting," *IEEE Access*, vol. 8, pp. 76433–76452, 2020.

[16] A. Ebrahimi, W. Withayachumnankul, S. F. Al-Sarawi, and D. Abbott, "Dual-mode behavior of the complementary electric-LC resonators loaded on transmission line: Analysis and applications," *J. Appl. Phys.*, vol. 116, no. 8, Aug. 2014, Art. no. 083705.
[17] A. Kapoor, P. K. Varshney, and M. J. Akhtar, "Microstrip line loaded simple ELC resonator sensor for dielectric characterization," in *IEEE MTT-S Int. Microw. Symp. Dig.*, Dec. 2019, pp. 1–4.
[18] P. K. Varshney, A. Kapoor, and M. J. Akhtar, "Highly sensitive ELC resonator based differential sensor," *IEEE Trans. Instrum. Meas.*, vol. 70, pp. 1–10, 2021.
[19] A. Karami-Horestani, F. Paredes, and F. Martín, "Phase-variation microwave displacement sensor with good linearity and application to breath rate monitoring," *IEEE Sensors J.*, vol. 23, no. 19, pp. 22486–22495, Oct. 2023.
[20] R. Shi, S. Yu, and N. Kou, "A miniaturized frequency-selective rasorber with absorption bands on two sides of passband for antenna dome," *IEEE Antennas Wireless Propag. Lett.*, vol. 21, pp. 2161–2165, 2022.
[21] B. J. Arritt, D. R. Smith, and T. Khraishi, "Equivalent circuit analysis of metamaterial strain-dependent effective medium parameters," *J. Appl. Phys.*, vol. 109, no. 7, Apr. 2011, Art. no. 073512.
[22] M. Yoo and S. Lim, "Polarization-independent and ultrawideband metamaterial absorber using a hexagonal artificial impedance surface and a resistor-capacitor layer," *IEEE Trans. Antennas Propag.*, vol. 62, no. 5, pp. 2652–2658, May 2014.
[23] S. N. Novin, S. Jarchi, and P. Yaghmaee, "Tunable frequency selective surface based on IDC-loaded electric-LC resonator incorporated with liquid crystal," in *Proc. Conf. Microw. Techn. (COMITE)*, Apr. 2017, pp. 1–4.
[24] H. Xiong and X.-M. Li, "Parametric investigation and analysis of an electric-LC resonator by using LC circuit model," *Appl. Comput. Electromagn. Soc.*, vol. 35, no. 10, pp. 1113–1118, Dec. 2020.
[25] J. Naqui and F. Martin, "Transmission lines loaded with bisymmetric resonators and their application to angular displacement and velocity sensors," *IEEE Trans. Microw. Theory Techn.*, vol. 61, no. 12, pp. 4700–4713, Dec. 2013.
[26] S. Harnsoongnoen and A. Wanthong, "Coplanar waveguide transmission line loaded with electric-LC resonator for determination of glucose concentration sensing," *IEEE Sensors J.*, vol. 17, no. 6, pp. 1635–1640, Mar. 2017.
[27] M. Stocchi, Z. Cao, C. H. Joseph, T. Voss, D. Mencarelli, L. Pierantoni, C. B. Kaynak, J. Hebeler, T. Zwick, M. Wietstruck, and M. Kaynak, "Gain enhancement of BiCMOS on-chip sub-THz antennas by mean of meta-cells," *Sci. Rep.*, vol. 12, no. 1, p. 3946, Mar. 2022.

C. H. JOSEPH (Member, IEEE) received the B.Sc. degree in physics from the St. John's College, Tirunelveli, India, in 2007, the M.Sc. degree in physics from The American College, Madurai, India, in 2010, and the Ph.D. degree in electronic engineering from the University of Rome "Tor Vergata," Rome, Italy, in 2016. He was a recipient of the "Marie Curie Fellowship" and an Early-Stage Researcher with the National Research Council (CNR-IMM), Rome, from 2013 to 2016. He was also an Institute Postdoctoral Fellow with the Department of Physics, Indian Institute of Technology (IIT) Madras, India, from 2017 to 2018. Since 2018, he has been a Researcher with the Department of Information Engineering, Polytechnic University of Marche (UnivPM), Ancona, Italy. His current research interests include nanoscale characterization of advanced materials and biological structures using scanning microwave microscopy (SMM) technique, nanoelectronics, microwave/millimeter wave, and sub-THz metamaterials device modeling and design.

D. MENCARELLI (Member, IEEE) received the Laurea degree in electronic and telecommunication engineering from the University Politecnica of Marche (UNIVPM), Ancona, Italy, in 2002 and 2005, respectively. Since 2014, he has been an Assistant Professor with the Department of Information Engineering, UNIVPM. His research interests include coherent charge transport in low dimensional systems, photonic crystals, nano-field effect transistors (nano-FET), planar slot array antennas and microwave components, scanning probe microscopy (SPM), optomechanics, and phononic devices. He is currently a member of the IEEE MTT'S Speaker Bureau, the Vice Chair of the MTT TC 8 Technical Committee "RF Nanotechnology," and an Associate Editor of the journals IEEE TRANSACTIONS ON NANOTECHNOLOGY and *Journal of Computational Electronics*.

L. PIERANTONI (Senior Member, IEEE) is currently a Full Professor in electromagnetic fields with the Polytechnic University of Marche (UnivPM), Ancona. His research interests include the investigation of the combined Maxwell-quantum transport phenomena in nano-materials/devices, the development of computational techniques for the multiphysics modeling of nano-to-meso-scale devices/systems, and atomistic (ab initio) simulations of novel and smart materials. He is also the Founder and the first Chair of the MTT-S RF Nanotechnology Technical Committee. He is also an IEEE MTT-S Distinguished Microwave Lecturer (DML) (2012–2014) and IEEE MTT-S DML Emeritus (2015–2016). He is also an IEEE Nanotechnology Council (NTC) Distinguished Lecturer (2015–2016). He is also an IEEE TRANSACTIONS ON NANOTECHNOLOGY (IEEE TNANO) Senior Editor. He is also the Vice-President of the NTC for the Educational Activities. He has got 12 European granted projects.

P. RUSSO (Senior Member, IEEE) received the Ph.D. degree in electronic engineering from the Polytechnic University of Bari, Bari, Italy, in April 1999.

From January 2005 to July 2019, she was an Assistant Professor with the Polytechnic University of Marche (UnivPM), Ancona, Italy, where she was appointed as an Associate Professor, in August 2020. She teaches antenna design and fundamental of electromagnetics. Her main research interests include the application of numerical modeling to EMC problems, antenna problems, plasma antennas, and electromagnetic sensors.

Dr. Russo is a member of Italian Electromagnetic Society (SIEm) and the Scientific Board of Italian Center for the study of the interactions between Electromagnetic Fields and Biosystem (ICEmB).

L. ZAPPELLI (Member, IEEE) received the M.S. (summa cum laude) and Ph.D. degrees in electronic engineering from the University of Ancona, Ancona, Italy, in 1986 and 1991, respectively. Since 1988, he has been with the Department of Information Engineering, Polytechnic University of Marche (UnivPM), Ancona, where he is currently an Assistant Professor. His research interests include microwaves, electromagnetic compatibility, phased array antennas, frequency selective surfaces, and microwave equivalent circuits.

Open Access funding provided by 'Università Politecnica delle Marche' within the CRUI-CARE Agreement